Reduced Band Gap Hybrid Perovskites Resulting from Combined Hydrogen and Halogen Bonding at the Organic−Inorganic Interface

Sebastien Sourisseau,[†] Nicolas Louvain,[†] Wenhua Bi,[†] Nicolas Mercier,*[,†] David Rondeau,[†] Florent Boucher,[‡] Jean-Yves Buzaré,[§] and Christophe Legein[§]

Laboratoire de Chimie, Ingénierie Moléculaire et Matériaux d'Angers, UMR-CNRS 6200, Université d'Angers, 2 Bd Lavoisier, 49045 Angers, France, Institut des Matériaux Jean Rouxel, UMR-CNRS 6502, Université de Nantes, 2 rue de la Houssinière, BP 32229, 44322 Nantes Cedex 3, France, Laboratoire des Oxydes et Fluorures, CNRS UMR 6010 and Laboratoire de Physique de l'Etat Condensé, CNRS UMR 6087, Institut de Recherche en Ingénierie Moléculaire et Matériaux fonctionnels, CNRS FR 2575, Université du Maine, Avenue Olivier Messiaen, 72085 Le Mans Cedex 9, France

Received October 5, 2006

Undistorted perovskite layers are formed in PbI_4-based hybrid perovskites incorporating $X-(CH_2)_2-NH_3^+$ (X = Br, Cl) cations. The outstanding structural feature of these compounds is the result of halogen and hydrogen bonding at the organic−inorganic interface, leading to the absence of hydrogen bonds between equatorial iodine atoms of the perovskite layer and ammonium parts, these last being located out of perovskite layers. As a consequence, these red salts display a reduced band gap (2.2 eV) which is assigned to a more disperse HOMO band compared to other salts such as $(I-(CH_2)_2-NH_3)_2PbI_4$.

Introduction

The large field of hybrid organic−inorganic compounds is continuously of high interest due to the opportunity to combine useful properties of both components, and the possibility to tune the physical properties thanks to small modifications at the organic−inorganic interface. Hybrid perovskites, which have the great advantage of being processed into thin films by room-temperature techniques such as spin-coating,[1] can possess semiconducting properties depending on the nature of the inorganic framework. Extensive work has been notably devoted to materials based on iodostannate perovskite layers which can be used as a semiconducting channel in thin-film field-effect transistors (TFTs),[2,3] with the potential of relatively high electrical mobility (0.6 $cm^2\ V^{-1}\ s^{-1}$ in $(C_6H_5C_2H_5NH_3)_2SnI_4$[2] for instance). This value nevertheless remains 2 orders of magnitude smaller than the one evidenced in $CH_3NH_3SnI_3$, which is a 3D perovskite with metallic conductivity.[4] Two main strategies have been considered to improve the charge carrier mobility of a given halogenometallate network: (1) to achieve hybrids with enhanced structural dimensionality, either multilayer perovskite materials[5] or materials with perovskite monolayers linked by covalent bridges;[6] (2) to tune the band gap associated with perovskite layers by incorporating selected cations which are able to impact the bonding features of the inorganic framework. In the last way, several results that relate the effect of steric interactions in organic sheets on the electronic properties of hybrids have been reported.[7] More recently, extended Hückel tight-binding band structure calculations on a series of idealized SnI_4 perovskite sheets indicate that the I−M−I bond angle is a dominant structural factor influencing the electronic structure of such organic−inorganic hybrid compounds.[8] In fact, the main interaction responsible for rotation and/or the tilt of $M^{II}X_6$ octahedra is the H bonding between ammonium parts and halide atoms. For instance, the change of hydrogen bonding during structural transitions which involves a change of geometrical characteristics of inorganic sheets results in thermochromism in some related materials.[9,10] It seems obvious that with restriction of the ammonium/halide interactions, as shown recently in the first example ($(HO-(CH_2)_2-NH_3)_2PbI_4$ salt),[10] less distorted perovskite layers could be obtained.

Herein, we first report on the preparation, X-ray structural characterization, optical absorption spectra, and electronic

* To whom correspondence should be addressed. Fax: 33.(2).41.73.54.05. Tel.: 33.(2).41.73.50.83. E-mail: nicolas.mercier@univ-angers.fr.
[†] Université d'Angers.
[‡] Université de Nantes.
[§] Université du Maine.

(1) (a) Mitzi, D. B. *Chem. Mater.* **2001**, *13*, 3283. (b) Mitzi, D. B. *J. Mater. Chem.* **2004**, *15*, 2355.
(2) Kagan, C. R.; Mitzi, D. B.; Chondroudis, K. *Science* **1999**, *286*, 945.
(3) Mitzi, D. B.; Chondroudis, K.; Kagan, C. R. *IBM J. Res. Dev.* **2001**, *45* (1), 29.
(4) Mitzi, D. B.; Field, C. A.; Schlesinger, Z.; Laibowitz, R. B. *J. Solid State Chem.* **1995**, *114*, 159.
(5) (a) Calabrese, J.; Jones, N. L.; Harlow, R. L.; Herron, N.; Thorn, D. L.; Wang, Y. *J. Am. Chem. Soc.* **1991**, *113*, 2328. (b) Mitzi, D. B.; Feild, C. A.; Harrison, W. T.; Guloy, A. M. *Nature* **1994**, *369*, 467. (c) Zhu, X. H.; Mercier, N.; Riou, A.; Blanchard, P.; Frère, P. *Chem. Commun.* **2002**, *18*, 2160.
(6) Mercier, N.; Riou, A. *Chem. Commun.* **2004**, *7*, 844.
(7) (a) Xu, Z.; Mitzi, D. B.; Dimitrakopoulos, C. D.; Maxcy, K. R. *Inorg. Chem.* **2003**, *42*, 2031. (b) Mitzi, D. B.; Dimitrakopoulos, C. D.; Kosbar, L. L. *Chem. Mater.* **2001**, *13*, 3728. (c) Xu, Z.; Mitzi, D. B.; Medeiros, D. R. *Inorg. Chem.* **2003**, *42*, 1400.
(8) Knutson, J. L.; Martin, J. D.; Mitzi, D. B. *Inorg. Chem.* **2005**, *44*, 4699.
(9) (a) Willet, R. D.; Hangen, J. A.; Lebsack, J.; Money, J. *Inorg. Chem.* **1974**, *13*, 2510. (b) Ishihara, T.; Takahashi, J.; Goto, T. *Solid State Commun.* **1989**, *69*, 933.
(10) Mercier, N.; Poiroux, S.; Riou, A.; Batail, P. *Inorg. Chem.* **2004**, *43*, 8361.

10.1021/cm062380e CCC: $37.00
Published on Web 01/11/2007

Table 1. Crystallographic Data for 1, 2a, 2b, and 3

	1 $(Cl-(CH_2)_2-NH_3)_2PbI_4$	**2a** α1-$(Br-(CH_2)_2-NH_3)_2PbI_4$	**2b** α2-$(Br-(CH_2)_2-NH_3)_2PbI_4$	**3** $(I-(CH_2)_2-NH_3)_2PbI_4$
Fw (g/mol)	875.86	964.78	964.78	1058.76
space group	*Pbnm*	*C*2/*c*	*Pbnm*	$P2_1/a$
a, Å	6.4703(2)	9.126(1)	6.4824(3)	8.753(1)
b, Å	12.839(7)	9.143(1)	12.9046(8)	8.747(1)
c, Å	20.797(2)	21.450(2)	21.141(2)	12.720(2)
α, deg	90	90	90	90
β, deg	90	98.65(1)	90	97.63(1)
γ, deg	90	90	90	90
V, Å^3	1727.7(5)	1769.4(3)	1768.5(2)	965.3(2)
Z	4	4	4	2
obs. reflns ($I > 2\sigma(I)$)/parameters	2027/66	1673/71	2597/66	1954/63
R1($I > 2\sigma(I)$)/wR2(all data)	0.039/0.098	0.041/0.103	0.039/0.089	0.034/0.103

structures of PbI_4-based hybrid perovskites incorporating $X-(CH_2)_2-NH_3^+$ (X = I, Br, Cl) bifunctional ammonium cations. In contrast with the PbI_4 layers found in the structure of $(I-(CH_2)_2-NH_3)_2PbI_4$ (**3**), almost undistorted perovskite layers are formed in structures of $(Cl-(CH_2)_2-NH_3)_2PbI_4$ (**1**) and α1- and α2-$(Br-(CH_2)_2-NH_3)_2PbI_4$ polymorphs (**2a** and **2b**, respectively), as a result of united halogen and hydrogen bonding at the organic−inorganic interface.

Experimental Section

Synthesis and Characterization. Starting materials $X-(CH_2)_2-NH_3^+X^-$, PbI_2, and concentrated HI in a 2/1/6 molar ratio were first added to acetonitrile (20 mL). The solution was then stirred a few minutes at room temperature, giving a clear yellow phase, and was then allowed to evaporate at room temperature. Platelike crystals of $(X-(CH_2)_2-NH_3)_2PbI_4$ (X = Br, Cl) were formed several hours later. The red crystals were collected by filtration and washed with cold ethyl acetate. [Anal. Calcd for $C_4N_2PbI_4Cl_2$ (**1**): C, 5.50; N, 3.20; Pb, 23.7; I, 58.0; Cl, 8.10. Found: C, 6.04; N, 3.17; Pb, 23.24; I, 57.31; Cl, 8.01. Anal. Calcd for $C_4N_2PbI_4Br_2$ (**2a** or **2b**) C, 4.97; N, 2.90; Pb, 21.45; I, 52.62; Br, 16.56. Found: C, 5.07; N, 2.86; Pb, 21.39; I, 51.42; Br, 15.85.] Starting from $Br-(CH_2)_2-NH_3^+$ entities, a mixture of **2a** and **2b** polymorph phases was obtained with a **2b**/**2a** ratio ranging from 0 to 0.5, which depends on the speed of evaporation. The crystals of **3** were obtained from a slow evaporation at room temperature for 1 week of a concentrated HI solution containing $Br-(CH_2)_2-NH_3^+Br^-$ and PbI_2 in a 2/1 ratio. Due to the large excess of iodide ions in the solution, the Br atoms on the ethyl groups of organic ligands were replaced by the atoms of I and resulted in the orange crystals of compound **3**. [Anal. Calcd for $C_4N_2PbI_6$: C, 4.53; N, 2.65; Pb, 19.6; I, 71.9. Found: C, 4.70; N, 2.61; Pb, 19.09; I, 70.98.] CPMAS $^1H-^{13}C$ solid-state NMR experiments which were carried out on **3** and (**2a** + **2b**) unambiguously confirm the presence of $I-(CH_2)_2-NH_3$ entities in **3** (see SI). Powder X-ray pattern of the three homogeneous samples showed that all reflections are indexed in the orthorhombic cell of **1**, and the monoclinic cells of **2a** and **3**, respectively. Thermogravimetric analysis measurements (TGA-2050 Instruments System), which consist of a 10 °C/min ramp from 25 to 900 °C under a flowing nitrogen atmosphere, show that compounds decompose in two steps with a first weight loss of 43.9% (**1**, $T = 150$ °C), 51.0% (**2a** + **2b**, $T = 210$ °C), 54.3% (**3**, $T = 200$ °C), which probably corresponds to the departure of $X(CH_2)_2NH_2$ and HX molecules (Calcd: 47.4% (**1**), 52.2% (**2a** or **2b**), 56.4% (**3**)), and the second weight loss at $T = 400$ °C corresponding to the sublimation of the MX_2 remaining salt. Differential scanning calorimetry (DSC) measurements were performed on a DSC-2010 TA Instruments system. For (**2a** + **2b**), the two endothermic peaks at $T = 107$ °C and $T = 153$ °C that are observed before the decomposition are assigned to a solid-state reaction between the organic cations and the inorganic network. This study will be reported in the near future.

Table 2. Selected Bond Distances (Å) and Angles (deg) for 1 ($(Cl-(CH_2)_2-NH_3)_2PbI_4$)[a]

Pb−I(3)	3.1722(6)	Pb−I(2)	3.2055(9)
Pb−I(1)#1	3.2019(8)	Pb−I(3)#2	3.2616(6)
Pb−I(1)	3.2019(8)	Pb−I(2)#3	3.2657(9)
I(1)#1−Pb−I(1)	174.255(19)	I(3)−Pb−I(2)	92.736(19)
I(3)−Pb−I(3)#2	173.149(11)	I(1)−Pb−I(2)	87.652(9)
I(2)−Pb−I(2)#3	178.07(3)	I(1)#1−Pb−I(3)#2	91.817(9)
I(3)−Pb−I(1)	88.461(9)	I(2)−Pb−I(3)#2	94.115(19)
I(3)−Pb−I(2)#3	89.191(18)	I(1)#1−Pb−I(2)#3	92.403(9)
I(3)#2−Pb−I(2)#3	83.957(18)		
Pb−I(2)−Pb#4	178.07(3)	Pb−I(3)−Pb#5	176.68(2)

[a] #1: $x, y, -z + 1/2$. #2: $-x + 1/2, y + 1/2, z$. #3: $x - 1, y, z$. #4: $x + 1, y, z$. #5: $-x + 1/2, y - 1/2, z$.

Table 3. Selected Bond Distances (Å) and Angles (deg) for 2a (α1-$(Br-(CH_2)_2-NH_3)_2PbI_4$)[a]

Pb−I(2)	3.1689(9)	Pb−I(1)#1	3.2187(8)
Pb−I(2)#1	3.1689(9)	Pb−I(1)#2	3.2410(8)
Pb−I(1)	3.2187(8)	Pb−I(1)#3	3.2410(8)
I(2)−Pb−I(2)#1	177.30(4)	I(1)−Pb−I(1)#1	91.40(3)
I(1)−Pb−I(1)#2	178.49(3)	I(1)#1−Pb−I(1)#2	90.099(9)
I(2)−Pb−I(1)	88.04(2)	I(2)−Pb−I(1)#2	91.86(2)
I(2)−Pb−I(1)#1	90.07(2)	I(1)#2−Pb−I(1)#3	88.40(3)
Pb−I(1)−Pb#4	178.49(3)		

[a] #1: $-x + 3, y, -z + 5/2$. #2: $x - 1/2, y - 1/2, z$. #3: $-x + 7/2, y - 1/2, -z + 5/2$. #4: $x + 1/2, y + 1/2, z$.

X-ray Crystallography. X-ray diffraction data of selected single crystals were collected on a Bruker-Nonius KAPPA-CDD diffractometer equipped with graphite-monochromated Mo Kα radiation ($\lambda = 0.71073$ Å). A summary of crystallographic data and refinement results for all compounds is listed in Table 1. Structures were solved and refined using the Shelxl97 package. Heavy atoms (Pb, I, Br, Cl) were first located using direct methods, C and N atoms then being located from the analysis of the Fourier difference maps. A statistical disorder affects the organic molecule in the structure of **2a**, the carbon atom bearing the halogen atom being located on two positions. The occupation rate of each position was first refined, agitation parameters being constrained to be equal, and was finally fixed to 0.5. All hydrogen atoms were treated with a riding model in all three structures. Positions and anisotropic displacement parameters of the non-H atoms were refined by full-matrix least-squares routines against F^2. Absorption effects were corrected using the Gauss method. Selected bond distances and angles for **1**, **2a**, **2b**, and **3** are provided in Tables 2−5. A complete list of crystallographic data, along with the atomic coordinates, the anisotropic displacement parameters, and bond distances and angles for each compound are given as Supporting Information.

Table 4. Selected Bond Distances (Å) and Angles (deg) for 2b (α2-(Br−$(CH_2)_2$−$NH_3)_2PbI_4$)[a]

Pb−I(3)	3.1798(8)	Pb−I(2)#2	3.2168(8)
Pb−I(1)#1	3.1858(6)	Pb−I(2)	3.2679(8)
Pb−I(1)	3.1858(6)	Pb−I(3)#3	3.2799(8)
I(1)#1−Pb−I(1)	175.37(2)	I(3)−Pb−I(2)	90.30(2)
I(2)#2−Pb−I(2)	176.92(3)	I(1)−Pb−I(2)	91.763(12)
I(3)−Pb−I(3)#3	175.104(12)	I(1)#1−Pb−I(3)#3	91.650(13)
I(3)−Pb−I(1)#1	88.494(13)	I(2)#2−Pb−I(3)#3	92.12(2)
I(3)−Pb−I(2)#2	92.78(2)	I(2)−Pb−I(3)#3	84.80(2)
I(1)#1−Pb−I(2)#2	88.320(12)		
Pb#4−I(2)−Pb	176.92(3)	Pb−I(3)−Pb#5	177.55(3)

[a] #1: $x, y, -z + 1/2$. #2: $x + 1, y, z$. #3: $-x + 3/2, y - 1/2, z$. #4: $x - 1, y, z$. #5: $-x + 3/2, y + 1/2, z$.

Table 5. Selected Bond Distances (Å) and Angles (deg) for 3 ((I−$(CH_2)_2$−$NH_3)_2PbI_4$)[a]

Pb−I(2)#1	3.1775(6)	Pb−I(1)	3.2225(5)
Pb−I(2)	3.1775(6)	Pb−I(1)#2	3.2243(5)
Pb−I(1)#1	3.2225(5)	Pb−I(1)#3	3.2243(5)
I(2)#1−Pb−I(2)	180.0	I(2)#1−Pb−I(1)#2	89.452(15)
I(1)#1−Pb−I(1)	180.0	I(2)−Pb−I(1)#2	90.548(15)
I(2)−Pb−I(1)#1	91.342(13)	I(1)#1−Pb−I(1)#2	87.668(9)
I(2)−Pb−I(1)	88.658(13)	I(1)−Pb−I(1)#2	92.332(9)
Pb−I(1)−Pb#4	147.379(15)		

[a] #1: $-x + 1, -y - 1, -z - 1$. #2: $-x + 1/2, y - 1/2, -z - 1$. #3: $x + 1/2, -y - 1/2, z$. #4: $-x + 1/2, y + 1/2, -z - 1$.

Optical Properties. Absorption spectra were measured on thin films for the most interesting compounds **1** and (**2a** + **2b**) or on powder for **3** using a Lambda 19 Perkin-Elmer spectrometer equipped with a Specac variable temperature cell P/N 21525 (vacuum environment). Crystallized films have been prepared by the spin-coating technique in the solvent of acetonitrile. The purity of the expected phases was provided by XRD patterns (ESI). It must be noted that the thin film of the bromine derivative is that of **2b**, although the starting samples contain both **2a** and **2b** polymorphs.

Electronic Band Structure Calculations. All calculations and geometry optimizations were carried out at the DFT level of theory using the PBE96 functional.[11] In the first step, to check the accuracy of the DFT/GGA approach to describe the electronic structure of these hybrid materials, structural optimizations have been done for the **1** and **3** compounds having respectively distorted and undistorted perovskite layers. Keeping experimental cell parameters, the internal atomic coordinates of all the atoms were adjusted, using VASP package[12] based on the efficient projected augmented wave (PAW) approach,[13] by minimizing Hellmann−Feynman forces. All calculations were converged with regard to the kinetic energy cutoff used for the plane wave (PW) basis set expansion and to the *k*-point density needed for the Brillouin zone integration. A cutoff of 500 eV and a ($6 \times 6 \times 4$) Monkhorst-Pack *k*-point mesh for **3** (($8 \times 4 \times 2$) for **1**) were sufficient to achieve convergence. Accuracy on the optimized bond lengths will be discussed later.

In a second step, electronic structure calculations for the density of states (DOS) and band dispersion analyses have been made on these optimized structures using the very accurate full potential linearized augmented plane wave (FLAPW) method, as embodied in the WIEN2K package.[14] This method is often used for the analysis as it allows an easier decomposition of the wave function into atomic-like orbitals. However, when one has to deal with small atomic radii like the C, N, and H atomic radii, the WIEN2k code is very computer-demanding. So only the inorganic part was introduced for the FLAPW calculation and various methods have been tested to simulate the charge transfer coming from the organic part (charged system, insertion of alkaline metals into the slab). The best agreement for the DOS and electronic gap between the VASP (complete structure) and FLAPW (inorganic part only) calculations was obtained by putting a sodium atom on the ammonium site. The electronic gaps were found to be 2.27 and 1.86 eV with WIEN2k for the iodine and chlorine compounds, respectively, compared to the 2.23 and 1.89 eV previously found with VASP. *k*-point meshes similar to previous ones were used. The PAW pseudopotential that has been chosen for the VASP calculations uses the following atomic configurations to describe the valence states: Pb($5d^{10}$ $6s^2$ $6p^2$), I($5s^2$ $5p^5$), Cl($3s^2$ $3p^5$), C($2s^2$ $2p^2$), N($2s^2$ $2p^3$), H($1s^1$). For the FLAPW calculation, an $R_{MT} \times K_{max} = 8.0$ was used to define the size of the basis set, using the same muffin tin radius ($R_{MT} = 1.58$ Å) for all the atoms.

Results and Discussion

Crystal Structures. The crystal structures of **1**−**3** are built up from sheets of corner-sharing PbI_6 octahedra alternating with organic cation bilayers. The degree of distortion of perovskite layers in terms of tilt of octahedra related to the mean equatorial PbI_2 plane can be easily visualized from Figures 1 and 2a: while no tilt occurs in **1**, **2a**, and **2b**, a quite strong tilt is observed in the structure of **3**. Another remarkable structural feature concerns the position of molecules between perovskite layers, and especially the position of ammonium parts: they clearly fit in the perovskite sheets in **3** (Figure 2a), and in contrast, they are protruded toward the interlayer space in **1**, **2a**, and **2b** (Figure 1). In the four structures, we can easily find that the carbon, halogen, and nitrogen atoms of molecules approximately lie in a plane. Nevertheless, considering the C−C bond of ethyl parts, the terminal substitutes, ammonium and halide groups, are either in trans conformation in the structure of **3** (Figure 2b) or in cis conformation in the structures of **1**, **2a**, and **2b** (Figure 1). The existence of two polymorphs, namely, α1-(Br−$(CH_2)_2$−$NH_3)_2PbI_4$ (**2a**) and α2-(Br−$(CH_2)_2$−$NH_3)_2PbI_4$ (**2b**), that are obtained together as synthetic products is quite original. There have been extensive studies reporting such systems that exhibit polymorphism. However, in contrast with our study, polymorphs resulted from temperature-dependent transitions (due to changes in the ordering or hydrogen bonding of the organic cations).[9,10,15] The structure of **2b** is isomorphous to that of **1**. The main difference between structures of both **2a** and **2b** polymorphs is the relative disposition of two consecutive organic bilayers along *c*: while molecular planes are all parallel to each other in **2b** (or in **1**, Figure 1a), molecular planes of cations belonging

(11) Perdew, J. P.; Burke, S.; Ernzerhof, M. *Phys. Rev. Lett.* **1996**, *77*, 3865.
(12) (a) Kresse, G.; Furthmüller, J. *Comput. Mater. Sci.* **1996**, *6*, 15. (b) Kresse, G.; Furthmüller, J. *Phys. Rev. B* **1996**, *54*, 11169.
(13) (a) Blöchl, P. E. *Phys. Rev. B* **1994**, *50*, 17953. (b) Kresse, G.; Joubert, D. *Phys. Rev. B* **1999**, *59*, 1758.
(14) Blaha, P.; Schwarz, K.; Madsen, G. K. H.; Kvaniscka, D.; Luitz, J. *An Augmented Plane Wave + Local Orbitals Program for Calculating Crystal Properties*; K. Schwarz: Techn. Universität Austria, 2001; ISBN 3-9501031-1-2.
(15) For example: (a) Chapuis, G.; Kind, R.; Arend, H. *Phys. Status Solidi A* **1976**, *36*, 285. (b) Chapuis, G. *Acta Crystallogr., Sect. B* **1978**, *34*, 1506. (c) Vacatello, M.; De Girolamo, M.; Busico, V. *J. Chem. Soc., Faraday Trans.* **1981**, *77*, 2367.

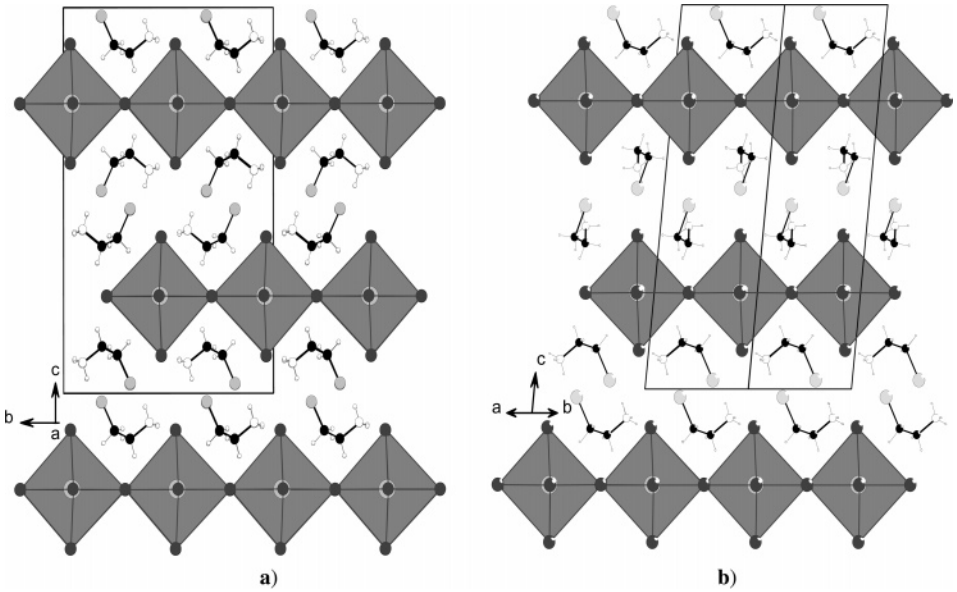

Figure 1. View of the layered hybrid perovskite structures of $(X-(CH_2)_2-NH_3)_2PbI_4$: (a) **1** (X = Cl); (b) **2a** (X = Br).

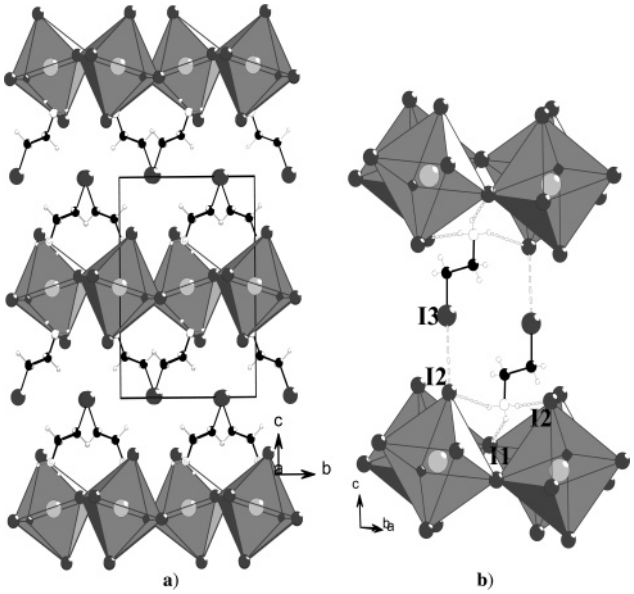

Figure 2. Structure of **3**: (a) general view down along *a*; (b) part of the layered structure showing hydrogen and halide interactions at the organic−inorganic interface.

to two consecutive organic bilayers are approximately perpendicular to each other in **2a** (Figure 1b).

The reasons for the different configurations of perovskite layers can be explained by an accurate examination of weak interactions in the organic bilayers or at the organic−inorganic interface. As is well-known, ammonium parts interact with halogen atoms of perovskite layers in two main ways, either with two bridging halogens and one terminal halogen (bridging halogen configuration) or with one bridging halogen and two terminal halogens (terminal halogen configuration),[16] as in **3** (Figure 2b). If the hydrogen bonding involves the rotation of corner-sharing MI_6 octahedra in the equatorial PbI_2 plan, the tilt of these polyhedra is mainly due to the position of the carbon fragment bearing the ammonium part. Thus, the strong tilt observed in **3** can be attributed to the position of ethyl parts which are located out of the inorganic sheet, the $C-NH_3$ bond being almost perpendicular to the layers (Figure 2). This situation is partly induced by the quite strong interaction between the iodine atom of the organic cations (I3) and the apical iodine atom of octahedra (I2). Please note that the distance of I3···I2 in compound **3** is 3.89(1) Å, which is less than twice the van der Waals radius of I (4.0 Å),[17] and the angle of C-I3···I2 equals 177.6(3)° (Figure 2b). The concept of halogen-bonding interaction, which was introduced by Dumas et al. in inorganic halogen complexes,[18] is found to be applied to the organic halogens.[19] The nature of halogen bonding is electrostatic interaction, and its origin consists of the anisotropy of the electron density around the organic halogen nucleus which can be represented by an ellipsoid elongated in the direction across the C−X bonding axis. Thus, the electron-deficient region in the vicinity of the halogen atom is the direction of maximum attractive electrostatic interaction toward electron-rich regions of Lewis bases (B). The stronger the halogen bonding is, the shorter the X···B distance will be, and the closer to 180° the angle of C−X···B bond will be. This is the real case for C-I3···I2 in **3**. It must be noted that there is no evidence of interaction involving the electron-rich region of I3 in the direction perpendicular to the C-I3 bond in **3**. Certainly due to steric considerations in the structure of **3**, the relative situation of molecules is completely different in the structures of **1**, **2a**, and **2b**. Figure 3 illustrates halogen and hydrogen interactions between perovskite layers in **2a**, only one position (C1A) of this disordered carbon atom being drawn (see Experimental Section). The distance of the halogen bonding between Br of the organic ligands and apical iodides (I2) is 3.652(3) Å,

(16) Mitzi, D. B. *Prog. Inorg. Chem.* **1999**, *48*, 1−121.

(17) Bondi, A. *J. Phys. Chem.* **1964**, *68*, 441.

(18) Dumas, J. M.; Gomel, L.; Guerin, M. *Molecular interactions involving organic halides. The chemistry of functional groups, supplement D*; Wiley: New York, 1983; pp 985−1020.

(19) Lommerse, J. P.; Stone, A. J.; Taylor, R.; Allen, F. H. *J. Am. Chem. Soc.* **1996**, *118*, 3108.

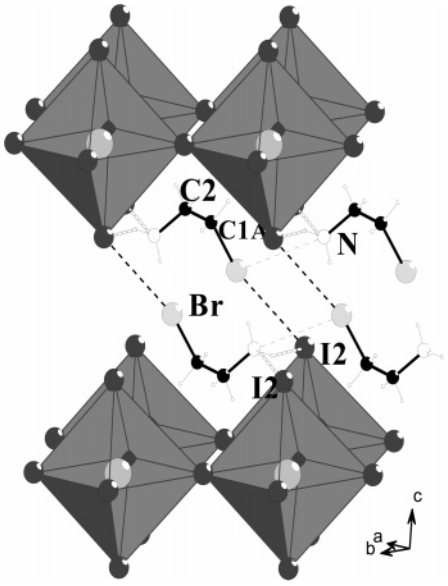

Figure 3. Part of the structure of **2a** showing hydrogen and halogen bonding at the organic−inorganic interface.

which is much less than the sum of R_{VDW}(I) and R_{VDW}(Br) (3.83 Å),[17] and the bond angle of C−Br···I2 is 152.7(8)°, comparatively far from 180°. As mentioned above, the original feature is the position of ammonium groups which are protruded in the interlayer space toward organic bromine (C−NH_3···Br bond angle of 161.6(8)°), and more accurately toward the electron-rich region of bromine, the C−Br···NH_3 bond angle being close to 90° (96.1(9)°) (Figure 3). While ammonium groups are located out of the perovskite sheet, the ethyl fragments of the ligands approximately lie in the apical iodide planes. Organic hydrogen atoms are certainly activated by the electron-withdrawing effect of both substitution groups, allowing weak C−H···$I_{equatorial}$ interactions (d((C1A)H···I1) = 3.090(3) Å). The three hydrogen atoms of primary ammonium are here bound in H···I_{apical} contacts: two quite strong interactions, (N−)H···I2: 2.74 and 2.83 Å shown in Figure 3, and a weaker one with an apical iodide of the neighboring perovskite layer ((N−)H···I2: 3.13 Å, not drawn in Figure 3). The absence of NH_3···$I_{equatorial}$ interaction and the position of ethyl fragments located in the perovskite sheets are undoubtedly the key points for the formation of undistorted perovskite layers in **2a** and **2b**. Similar relative disposition of cations and interactions between X and ammonium groups are observed in **1**, with nevertheless a weaker halogen bonding, as expected for an organic chlorine compared to organic bromine or organic iodine atoms. The different geometrical characteristics noticed above for the bromine compound are for **1**: d(Cl···I_{apical}) = 3.798(3) Å (to be compared to R_{VDW}(I) + R_{VDW}(Cl) = 3.73 Å), C−Cl···I_{apical} bond angle 159.0(8)°, C−NH_3···Cl bond angle 161.3(5)°, C−Cl···NH_3 bond angle 99.1(3)°, (N−)H···I_{apical}: 2.75, 2.76, and 3.017(3) Å, d((C_{ethyl})H···$I_{equatorial}$) = 3.197(2)Å. As shown in Figure 4, it is easy to find the great difference between two kinds of inorganic layers constructed by corner-sharing PbI_6 octahedra. In **3**, strong distortion is observed with an $I_{equatorial}$−Pb−$I_{equatorial}$ bond angle of 147.4°, whereas this bond angle is exceptionally close to 180° in **1**, **2a**, and **2b** (176.9−178.5° range, see Tables 2−5). Except for a 2,2′-biimidazolium lead(II) iodide compound, the highest $I_{equatorial}$−Pb−$I_{equatorial}$ bond angle reported up to now in several iodometallate hybrid perovskites is close to 160°.[7,10,20] In the 2,2′-biimidazolium salt, the quite undistorted perovskite layers (173.7° $I_{equatorial}$−Pb−$I_{equatorial}$ bond angle) are nevertheless built up from irregular PbI_6 octahedra (dPb−I in the 3.10−3.36 Å range, I−Pb−I bond angle (adjacent iodides) in the 79.9−94.2° range), revealing stereoactivity of 6s lone-pair electrons of lead(II) atoms.[21] In contrast, the geometry of the PbI_6 unit is close to the ideal octahedron in **1** (dPb−I in the range 3.17−3.26 Å, I−Pb−I bond angle in the range 84.0−94.1°), **2a** and **2b** (dPb−I in the range 3.17−3.24 Å (**2a**) and 3.18−3.28 Å (**2b**); I−Pb−I bond angle in the range 88.0−91.9° (**2a**) and 84.8−92.8°(**2b**), see Tables 2−4).

Optical Properties and Electronic Structures. Such hybrid materials have an exciton state, associated with the band gap of the inorganic layers, in their electronic structure, giving a sharp peak in the corresponding optical absorption spectra even at room temperature.[9b,22] The room-temperature UV−Vis absorption spectra of (X−$(CH_2)_2$−$NH_3)_2PbI_4$ (as thin films for **1** and **2b**; or powder for **3**, see Experimental Section) are shown in Figure 5. The exciton peak arises at λ = 545 nm and λ = 550 nm for **1** and **2b**, respectively, which constitutes the highest observed values for PbI_4-based perovskites. This red shift of the exciton peak compared to usual situations, as illustrated for the X = I compound (λ = 505 nm), indicates a reduced band gap in corresponding salts. The correlation between the band gap and the bonding features of perovskite layers (MX_6 octahedra distortion, stereoactivity of ns lone-pair electrons on Pb^{II} (n = 6) or Sn^{II} (n = 5) atoms, X−M−X bond angles) has been established from the careful analysis of several crystal structures of hybrids.[7] More recently, extended Hückel tight-binding band structure calculations on a series of idealized SnI_4 perovskite sheets reveal that the I−M−I bond angle is a dominant structural factor influencing the band gap.[8] The two experimental borderline cases (X−$(CH_2)_2$−$NH_3)_2PbI_4$ (**1**, **2a**, or **2b**) and (I−$(CH_2)_2$−$NH_3)_2PbI_4$ (**3**), in terms of distortion of perovskite layers, were especially well-suited to estimate the effect of distortions of the $M^{II}X_4$ perovskite layers on the electronic structures of related compounds **1** and **3**.

Before discussing in detail the electronic structure of the **1** and **3** compounds, we better have a look at the optimization results in advance. Concerning the organic ligand, structural optimization for the hydrogen positions based on DFT is successful. The resultant bond lengths are d(C−H)$_{ave}$ = 1.10 Å and d(N−H)$_{ave}$ = 1.04 Å. The C−C and C−N distances (1.51 and 1.50 Å, respectively) or Cl−C and I−C distances (1.80 and 2.16 Å, respectively) are properly co-incident with the experimental ones. According to the bond lengths of the iodine compound (d(Pb−I_{eq})$_{ave}$ = 3.25 Å and d(Pb−I_{ap})$_{ave}$ = 3.21 Å) and the chlorine compound (d(Pb−I_{eq})$_{ave}$ = 3.23 Å and d(Pb−I_{ap})$_{ave}$ = 3.20 Å), the results of DFT optimiza-

(20) Mitzi, D. B. *Chem. Mater.* **1996**, *8*, 791.
(21) Tang, Z.; Guan, J.; Guloy, A. M. *J. Mater. Chem.* **2001**, *11*, *479.*
(22) Ishihara, T.; Takahashi, J.; Goto, T. *Phys. Rev. B* **1990**, *42*, 11099.

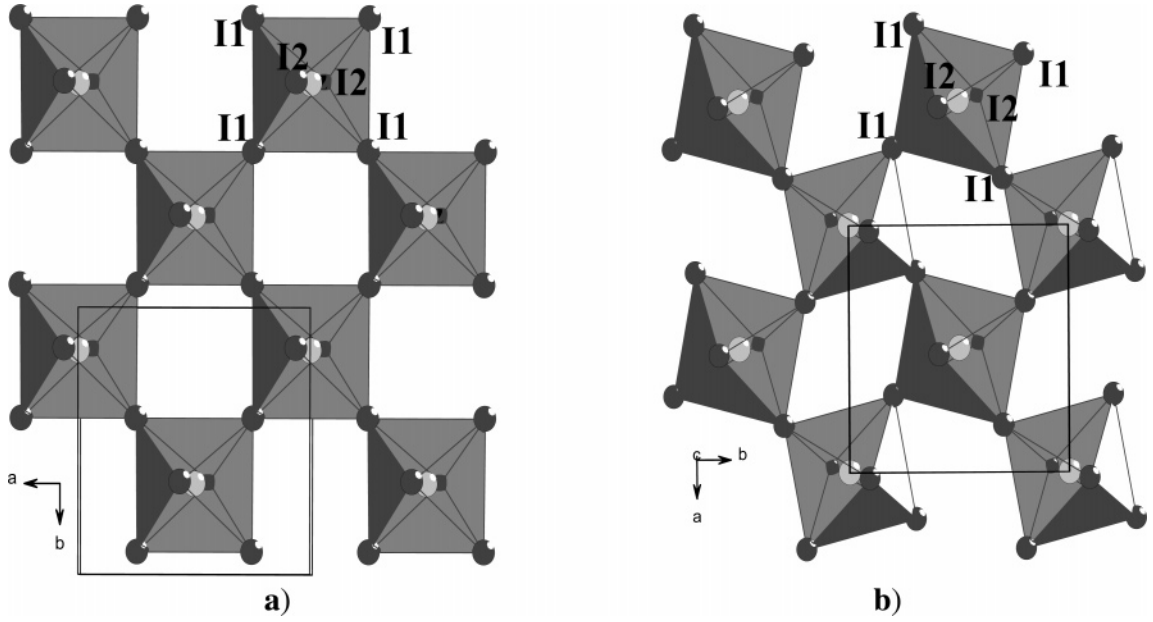

Figure 4. PbI_4^{2-} perovskite layer: (a) in **2a**; (b) in **3**.

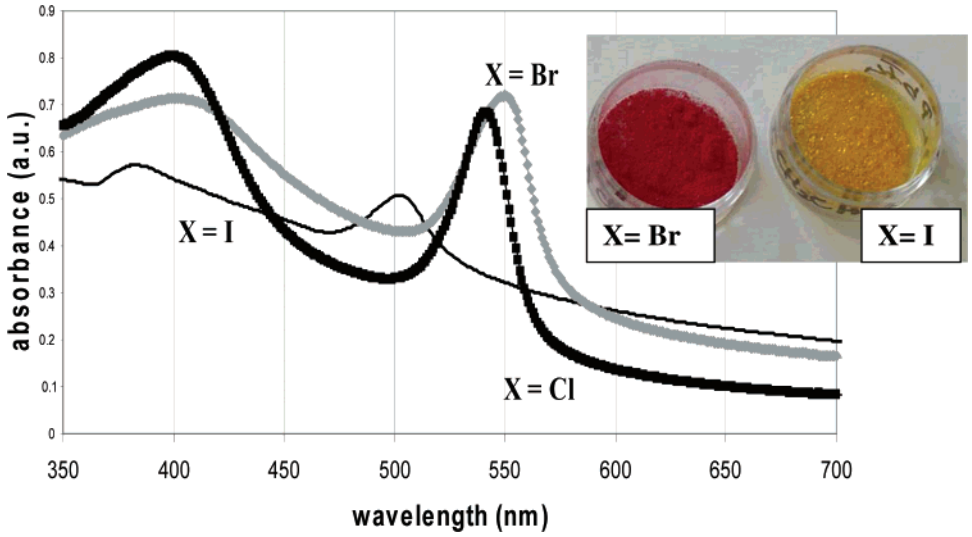

Figure 5. Room-temperature UV−Vis spectra of $(X-(CH_2)_2-NH_3)_2PbI_4$ (350−700 nm range), the exciton peak arising at $\lambda = 550$ nm (X = Br, **2b**), $\lambda = 545$ nm (X = Cl, **1**), and $\lambda = 505$ nm (X = I, **3**), and red and orange samples of (**2a** + **2b**) and **3** (photo).

tion are also satisfying. On average, the deviation compared to the experimental value is less than 1% for the bond distances for each part.

It is not so easy to discuss the correct description of the interactions between the organic and inorganic parts as the accuracy on the H positions obtained from X-ray diffraction is very low. Nevertheless, all the hydrogen bonds described above are well-reproduced after the structural relaxations. Looking at the halogen bonds, the distances are also reproduced very well by the calculations: d(I···I) = 3.78 Å and d(Cl···I) = 3.79 Å with, however, a small underestimation of 3% for the I···I bond length (observed 3.89(1) Å). In summary, according to this bond distance analysis and to the inspection of bond angles (not described here), we believe the DFT calculations are accurate enough to correctly reproduce the structural features of these hybrid perovskites and that reliable parameters could be extracted from the band structure analysis.

The curves of DOS for **1** and **3** and respective band structures calculated along high-symmetry lines are shown in Figure 6 (see Bradley and Cracknell for the labels).[23] The evolution of the calculated electronic gap corresponds to what is expected from experiment: 1.9 eV for the undistorted perovskite layer (chlorine compound, observed 2.2 eV) and 2.3 eV for the distorted perovskite layer (iodine compound, observed 2.45 eV). The difference between experiments and DFT is a classical problem of this ground state theory, as already mentioned by Chang et al.[24] For **1** and **3**, the band edge states come mainly from the inorganic PbI_4 layer, while the highest occupied levels and the lowest unoccupied levels

(23) Bradley, C. J.; Cracknell, A. P. *The Mathematical Theory of Symmetry in Solids*; Clarendon: Oxford, 1972.
(24) Chang, Y. H.; Park, C. H.; Matsuishi, K. *J. Korean Phys. Soc.* **2004**, *42*, 889.

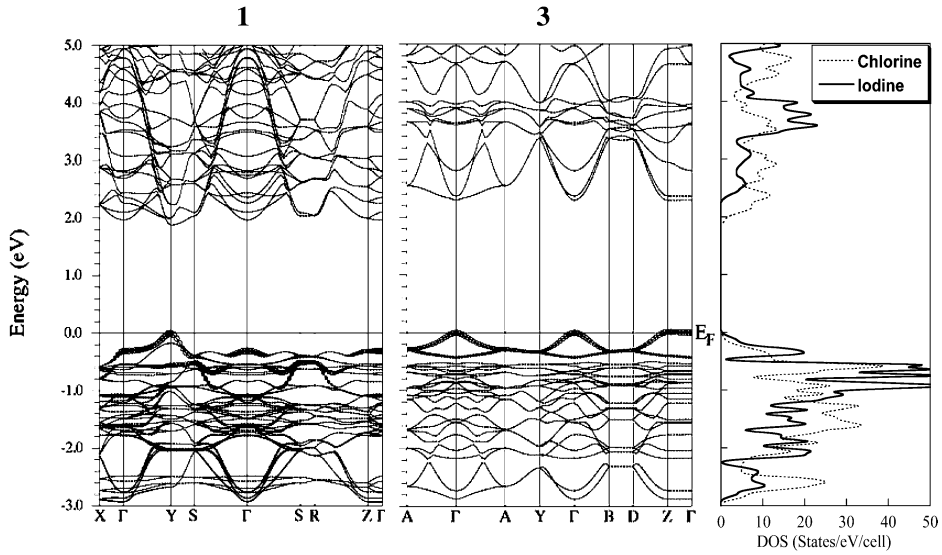

Figure 6. Band structure of the **1** and **3** compounds calculated with the FLAPW method and corresponding DOS on the right part. The contribution of the Pb 6s levels into the wave function is shown as fat bands evolution.

of the organic part are located around −3.5 eV below E_F and around 3.5 eV above E_F, respectively. A very precise analysis of the band structure of layered perovskite was provided by Knutson et al.[8] The band structures calculated in our work resemble a lot the extended Hückel band structure given by these authors. We give here the main features.

The perovskite layer can be formally considered as a charged $(PbI_4)^{2-}$ sheet with the +2 and −1 oxidations states for lead and iodine atoms, respectively. So the conduction band (CB) is formed by the empty Pb 6p bands, the p_x and p_y orbitals being highly dispersed in the Brillouin zone due to an antibonding interaction with the iodine 5p states. The valence band (VB) comes mainly from the I 5p band and the covalent-bonding interaction between the Pb 6p and the I 5p states is responsible for the stabilization of the states below −2.5 eV. One should remember that the number of atoms in the undistorted cell is twice the number of atoms of the distorted one. So the number of bands is double for compound **1**. The states of the Na atoms introduced between sheets to mimic the charge transfer appear as rather flat levels around 3.8 eV. Those levels do not present any covalent interactions with the other PbI_4 levels.

For both calculations, a direct band gap is observed between nonbonding lead p_x/p_y states into the CB and, into the VB, p states of iodine strongly mixed with the Pb 6s states. The Pb 6s character is expressed as a fat band (width of circles proportional to the wave function character), which appears distinctly at the top of the VB (Figure 6), the main part of the Pb 6s being around −7 eV. This Pb 6s/I 5p interaction is an antibonding one that disperses the iodine p states and push the last occupied band at higher energy. An isosurface drawing of the charge density corresponding to these last occupied states is shown in Figure 7 for both compounds. Thus, the larger the overlap is between the Pb 6s/I 5p states, the stronger the band dispersion. For the distorted layer, the overlap is less than that in the undistorted one. As a consequence, the Pb 6s character appears in a smaller energy range (≈0.4 eV) for the distorted layer compared to roughly 0.8 eV for the undistorted one. This is coherent with the band gap reduction as explained by Knutson et al.,[8] if the bottom of the CB (nonbonding Pb p_x/p_y states) is taken as a reference. A more disperse band, as found in the case of the regular sheet, will correspond to a smaller DOS at the top of the VB (Figure 6) and consequently a smaller effective mass. Thus, higher charge carrier mobility is expected for the regular layer compared to the distorted one.

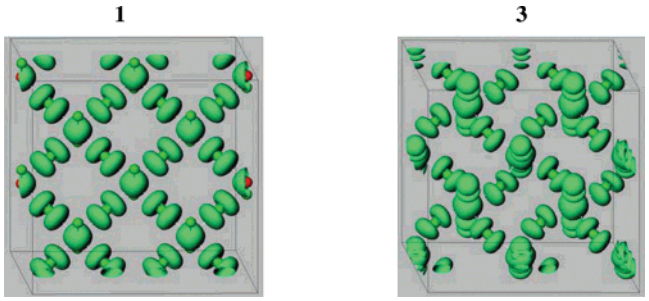

Figure 7. Isosurface of the charge density corresponding to the last occupied states for the **1** and **3** compounds and showing the antibonding interactions between the iodine 5p states and the lead 6s orbitals.

Conclusion

In summary, in the structures of $(X-(CH_2)_2-NH_3)_2PbI_4$ (X = I, Br, Cl), the $X-(CH_2)_2-NH_3^+$ bifunctional cations involve two supramolecular interactions never combined in $(RNH_3)_2MX_4$ layer perovskite structures, N−H···X− hydrogen bonding, and C−Y···X− halogen bonding. In $(X-(CH_2)_2-NH_3)_2PbI_4$ (X = Cl, Br), the united effect of these weak interactions at the organic−inorganic interface results in the formation of undistorted PbI_4 perovskite layers (Pb−I−Pb bond angles close to 180 °C) consisting of corner-sharing regular octahedra. As a consequence, these red salts display a reduced band gap (2.2 eV). According to the results of electronic structure calculations, this reducedband gap is

assigned to a more disperse HOMO band compared to other salts based on conventional perovskite layers as in $(I-(CH_2)_2-NH_3)_2PbI_4$ and is greatly beneficial to the mobility.

Acknowledgment. The calculation presented in this work has been carried out at the "Centre Régional de Calcul Intensif des Pays de la Loire" (CCIPL), financed by the French Research Ministry, "the Région Pays de la Loire", and Nantes University. We thank Pays de la Loire region for a post-doc fellowship to W.B.

Note Added after ASAP Publication. Additional information was added to section 8 of the Supporting Information file (PDF) published ASAP January 11, 2007; the corrected version of the Supporting Information was published ASAP January 18, 2007.

Supporting Information Available: Crystallographic data: single-crystal results (CIF) and powder X-ray patterns for **1**, **2a**, **2b**, and **3**, thermal analysis (TGA, DSC), and CPMAS $^{1}H-^{13}C$ solid-state NMR (**2a** + **2b**, **3**). This material is available free of charge via the Internet at http://pubs.acs.org.

CM062380E